Journal of Visualization, Vol. 10, No. 1 (2007)21-24

Review Report

Flow Visualization of Bubble Collapse Flow

Jaw, S. Y.*[1], Chen, C. J.*[2], and Hwang, R. R.*[1]

*1 Department of System Engineering and Naval Architecture, National Taiwan Ocean University, Keelung, Taiwan, R.O.C. E-mail: syjaw@ntou.edu.tw
*2 College of Engineering, Florida A&M University – Florida State University, Tallahassee, Florida, U.S.A.

Received 13 October 2006

1. Introduction

The flow induced by bubble collapse has been investigated for a long time, mainly motivated by the urge to understand the cavitation phenomena (Vogel et al., 1989), and the applications on the surface cleaning, metal hardening, or the micro fusion, etc. The collapse of cavitation bubbles formed in the liquid due to the occurrence of vapor pressure can lead to the production of liquid jets and shock waves. Detailed characteristics of the bubble collapse flow, such as the velocity and pressure distributions, are required for engineering applications. However, they are not easy to be measured, since the bubbles are small in size, generally micro meters to millimeters, and collapse in a very short time, measured in micro seconds. Experimental studies of the bubble collapse flow using high speed photography have been reported (Kodama and Tomita, 2000; Brown and Williams, 2000). Most of them have provided only the qualitative flow characteristics, due to the limitation of the recording devices. Both the frame transfer rate and the image resolution of the recording devices are not high enough to reveal the detailed characteristics of the bubble collapse flow.

It is known that the time scale of the bubble collapse is proportional to the square root of the bubble diameter. A large scale bubble provides better temporal and spatial resolution, which makes the detailed measurements of bubble collapse flows easier. Measurements of the break-up of a large, inflated rubber balloon in deep water were reported (Lawson et al., 1999). Experimental and computational results obtained were well in agreement; however, the rubber balloon is not formed by surface tension. Therefore, the balloon collapse flow can be quite different from the flow induced by the collapse of the bubble formed by surface tension. Alternatively, soap bubble is a better choice to perform the initiative analysis of the bubble collapse flow, since soap bubbles are formed by surface tension. The pressure inside the soap bubble is known to be $\Delta p = 4\sigma / R_{\max}$ higher than the surrounding atmosphere. In addition, soap bubbles can be easily generated to the size fit for the experiments. The effects of the surface tension and the pressure gradient to the bubble collapse flow can be clearly manifested. Flow visualization analyses of soap bubble collapse flow are thus performed in this study.

2. Experimental Setup

An injector was dipped in the 1.5% Ivory liquid soap solution to generate soap bubbles. Inside the soap bubbles were smoke particles in size $2\,\mu m$, generated from Shell Ondina 17 oil. For each experiment run, a soap bubble was placed on a ring support, and closed in a chamber to reduce the interference of the surrounding air. A needle on top of the bubble was triggered by a synchronized signal generated from the PIV system to pierce and break the soap bubble.

The bubble collapse flow was illuminated by two Nd-Yag pulse laser sheets triggered sequentially with 1/10,000 second time delay in between. Two sequential particle images were recorded using a double exposure mode PIV camera, with a resolution of 1360 by 1036 pixels. To clearly manifest the characteristics of the bubble collapse flow, part of the experiments were performed using color dye lasers (Jaw and Wu, 2000). Pulsed laser sheets in two different colors, red and green, were used to illuminate the flow field. Two colored, multiple exposure particle images were recorded by a color 3-CCD camera, with a resolution of 640 by 480 pixels. The system setup is

shown in Fig. 1.

With two sequential images available, the magnitude and direction of the velocity vectors can be determined using cross correlation analysis. A modified pattern matching correlation scheme developed in house, with multi-pass, window offset, central difference (Wereley and Meinhart, 2001), and Gaussian weighting (Florio et al., 2002), was used to calculate the velocity distribution. Complete velocity fields were obtained with the stray velocities removed, and then filled with second order interpolation scheme.

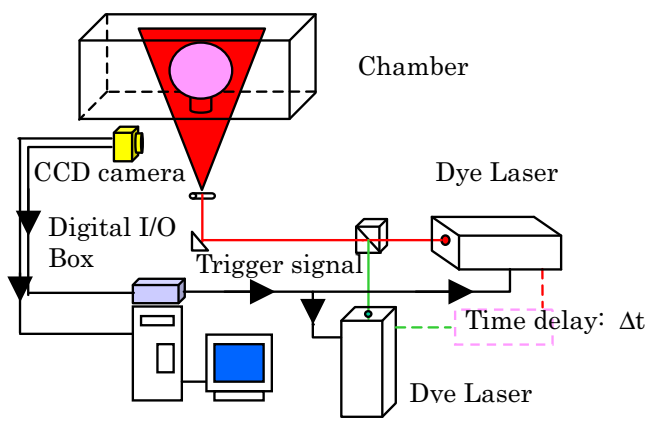

Fig. 1. PIV system for bubble collapse flow.

3. Results and Discussion

The flow induced by a partially collapsed soap bubble of diameter 4.86 cm (volume 60 c.c.) is shown in Fig. 2. It is found that a series of the Kelvin-Helmholtz vortices, which arise in shear flow along a contact discontinuity, are formed around the bubble sphere. A color image recorded with smoke filled both inside and outside of the bubble, as shown in Fig. 3, manifests the formation of the Kelvin-Helmholtz vortices more clearly.

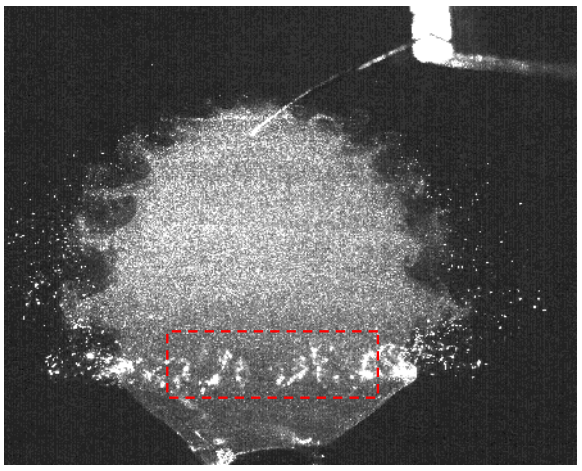

Fig. 2. Partially collapsed soap bubble.

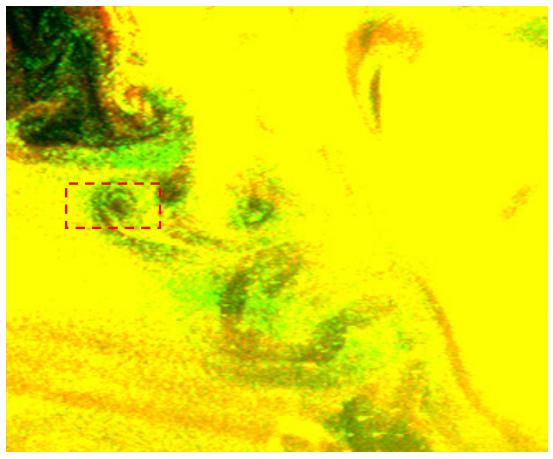

Fig. 3. Formation of Kelvin-Helmholtz vortices.

When the bubble collapsed, the pressure inside was gradually released. Smaller pressure and larger velocity occurred on the edge of the bursting rim due to the pressure release. The vortices are tilted downward, due to the continuous shearing motion of the bursting rim. Surrounding fluids then entrained and formed another vortex at the root of the Kelvin-Helmholtz vortex, as marked in Fig. 3. Rippling instability exists around the bursting rim, as marked by the red rectangle in Fig. 2. The rippling instability from the top view of a half-collapsed bubble is shown in Fig. 4. Higher smoke density in the bubble center of Fig. 4 implies that a convergent jet is developed during the bubble collapse, which will be more clearly manifested in the quantitative analysis discussed later on.

The soap film of the soap bubble is thinner on the top and thicker on the bottom, due to the gravity effect. The bursting velocity is not a constant, but varies with the thickness of the soap film. To manifest the thickness influence, a soap bubble was setup horizontally, with the support ring on the right and the needle on the left. The bubble was pierced through the left. The thinner film on the top bursts faster than the thicker film on the bottom, as shown in Fig. 5.

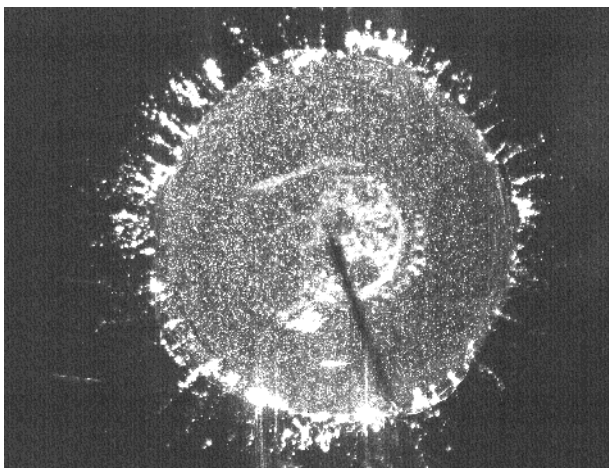

Fig. 4. Top view of partially collapsed bubble.

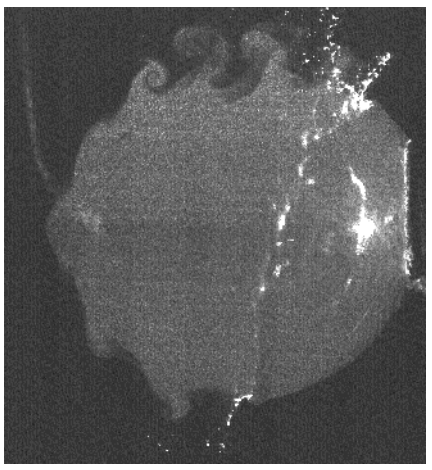

Fig. 5. Horizontally setup bubble collapse flow.

The elapsed time for a bubble with a diameter of 4.86 cm to completely collapse is about 0.0075 seconds. The bursting velocity, estimated by dividing half of the circumference of the bubble by the collapsing time, is about 10.18 m/s. The speed of disturbance transmitted on a two-dimensional soap film in the atmosphere is estimated to be 2.5 m/s to 3.7 m/s (Wen et al., 2004), depending on the thickness of the soap film. The pressure inside the soap bubble is $\Delta p = 4\sigma / R_{\max}$ higher than the surrounding atmosphere, where σ is the surface tension of the soap film, and $R_{\max}$ is the radius of the soap bubble. The bursting velocity is accelerated by the pressure difference, such that it is much faster than the disturbance transmitted on the soap film. Together, the pressure difference and the shearing effect of the bursting rim generate the series of Kelvin-Helmholtz vortices around the bubble sphere.

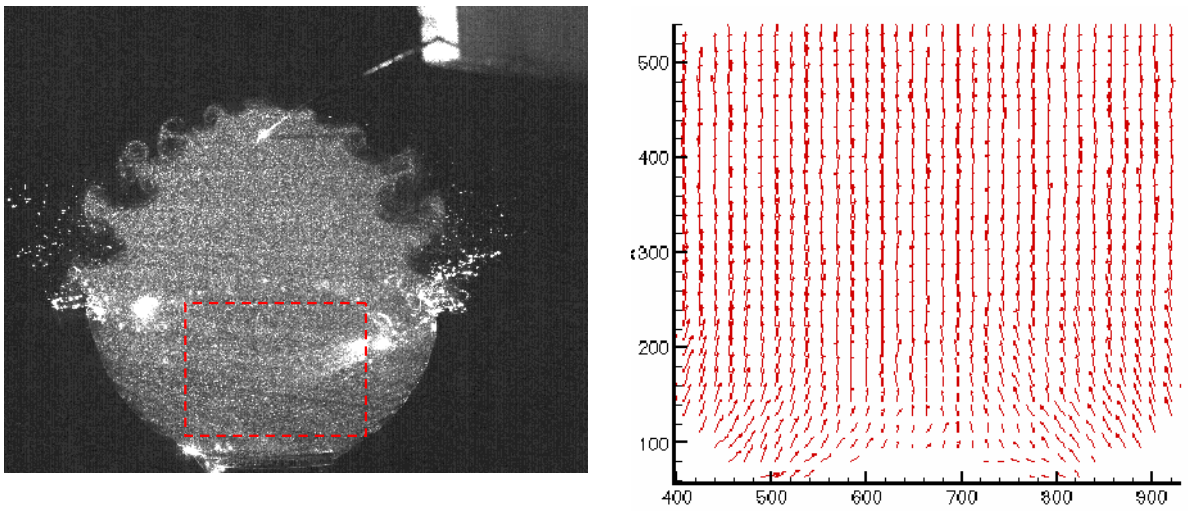

(a) Image of half collapsed bubble (b) Velocity vectors

Fig. 6. Measurements of a half collapsed soap bubble.

To perform the quantitative analysis, two sequential images were recorded using a double exposure mode PIV camera for each experiment run. The time interval between the two images is 1/7500 of a second. When the bubble collapsed, the pressure release from the bubble will induce the upward moving motion of the fluid. Favorable pressure gradients toward the central axis of the bubble are induced due to the pressure release, which in turn will push the fluid to move toward the central axis of the bubble. A convergent jet is thus formed. The marked area of Fig. 6(a) and its corresponding velocity vector distribution, shown in Fig. 6(b), clearly manifests such a convergent flow.

The streamline patterns for the different stages of a bubble collapse flow are presented in Fig. 7. As the bubble collapse proceeds from top to bottom, the curvature inside the bubble changes from convex to concave. Due to the curvature change and the pressure release inside the bubble, the streamline patterns evolve from the converged pattern, to the parallel pattern, to the pattern with a expanded middle, as shown in Figs. 7(a), 7(b), and 7(c). As the bubble is fully collapsed, the swell

effects, due to the pressure release, will induce a favorable pressure gradient underneath, causing the surrounding fluids to be sucked in toward the central axis. A saddle point, where the vertical outgoing streamlines and the horizontal incoming streamlines meet, then occurs near the bottom of the bubble, as shown in Fig. 7(d).

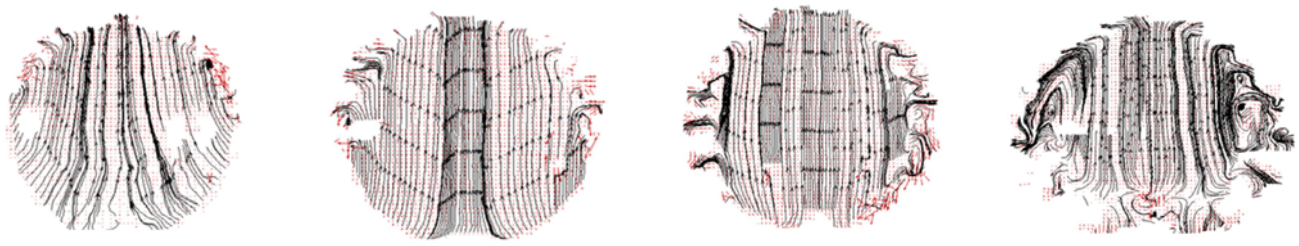

(a) 1/4 collapsed (b) Half collapsed (c) 3/4 collapsed (d) Fully collapsed

Fig. 7. Streamline patterns of bubble collapsed flow.

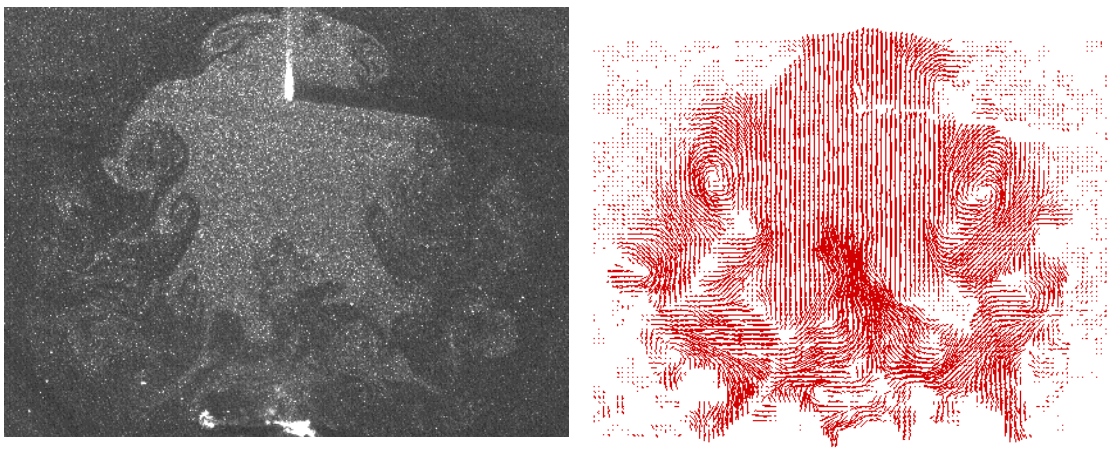

(a) Image of fully collapsed flow (b) Velocity vectors

Fig. 8. Soap bubble fully collapsed flow.

The image and the calculated velocity vectors of a fully collapsed bubble flow are shown in Fig. 8. The vortices and the convergent jet of the complicated flow are all successfully measured.

References

Brown, S. W. J. and Williams, P. R., An experimental study of liquid jets formed by bubble-shock wave interaction in dilute polymer solutions, Experiments in Fluids, 29 (2000), 56-65.

Florio, D. Di, Felice, F. Di, and Romano, G. P., Windowing, re-shaping and re-orientation interrogation windows in particle image velocimetry for the investigation of shear flows, Measurement Science and Technology, 13 (2002), 953-962.

Jaw, S. Y. and Wu, J. L., The alternating color image anemometry and its application, Journal of Flow Visualization, 7-3 (2000), 105-122.

Kodama, T. and Tomita, Y., Cavitation bubble behavior and bubble-shock wave interaction near a gelatin surface as a study of in vivo bubble dynamics, Applied Physics B, 70 (2000), 139-149.

Lawson, N.J., Rudman, M., Guerra, A., and Liow, J. L., Experimental and numerical comparisons of the break-up of a large bubble, Experiments in Fluids, 26-6 (1999), 524-534.

Vogel, A., Lauterborn, W. and Timm, R., Optical and acoustic investigations of the dynamics of laser-produced cavitation bubbles near a solid boundary, Journal of Fluid Mechanics, 206 (1989), 209-338.

Wen, C. Y., Chang-Jian, S. K. and Chuang, M. C., Analogy between soap film and gas dynamics, II. Experiments on one-dimensional motion of shock waves in soap films, Experiments in Fluids, (2002) DOI 10.1007/s00348-002-0540-6.

Wereley, S. T. and Meinhart, C. D. Second-order accurate particle image velocimetry, Experiments in Fluids, 31-3 (2001), 258-268.

Author Profile

Ching – Jen Chen: He serves as the Dean of Engineering at Florida A&M University-Florida State University College of Engineering. He received his PhD in Mechanical Engineering from Case Western Reserve University in 1967. He received Alexander von Humboldt U.S. Senior Scientist award in 1974. His field of interest is biomedical engineering and flow visualization, turbulent flow, convective heat transfer and nano magnetic materials. He is a life fellow of ASME and fellow of ASCE. He has supervised 37 doctoral dissertations and 32 master theses. Currently he serves as U.S. Regional Editor for Journal of Visualization.